Clin Oral Invest (2016) 20:1271–1278
DOI 10.1007/s00784-015-1606-1

ORIGINAL ARTICLE

Multifractal spectrum and lacunarity as measures of complexity of osseointegration

Daniel de Souza Santos[1] · Leonardo Cavalcanti Bezerra dos Santos[2] · Alessandra de Albuquerque Tavares Carvalho[2] · Jair Carneiro Leão[2] · Claudio Delrieux[3] · Tatijana Stosic[4] · Borko Stosic[4]

Received: 21 January 2015 / Accepted: 21 September 2015 / Published online: 6 October 2015

Abstract
Objectives The goal of this study is to contribute to a better quantitative description of the early stages of osseointegration, by application of fractal, multifractal, and lacunarity analysis.
Materials and methods Fractal, multifractal, and lacunarity analysis are performed on scanning electron microscopy (SEM) images of titanium implants that were first subjected to different treatment combinations of i) sand blasting, ii) acid etching, and iii) exposition to calcium phosphate, and were then submersed in a simulated body fluid (SBF) for 30 days. All the three numerical techniques are applied to the implant SEM images before and after SBF immersion, in order to provide a comprehensive set of common quantitative descriptors.
Results It is found that implants subjected to different physicochemical treatments before submersion in SBF exhibit a rather similar level of complexity, while the great variety of crystal forms after SBF submersion reveals rather different quantitative measures (reflecting complexity), for different treatments. In particular, it is found that acid treatment, in most combinations with the other considered treatments, leads to a higher fractal dimension (more uniform distribution of crystals), lower lacunarity (lesser variation in gap sizes), and narrowing of the multifractal spectrum (smaller fluctuations on different scales).
Conclusion The current quantitative description has shown the capacity to capture the main features of complex images of implant surfaces, for several different treatments. Such quantitative description should provide a fundamental tool for future large scale systematic studies, considering the large variety of possible implant treatments and their combinations.
Clinical relevance Quantitative description of early stages of osseointegration on titanium implants with different treatments should help develop a better understanding of this phenomenon, in general, and provide basis for further systematic experimental studies. Clinical practice should benefit from such studies in the long term, by more ready access to implants of higher quality.

Keywords Dental implants · Osseointegration · Fractal dimension · Multifractal spectrum · Lacunarity

✉ Borko Stosic
borko@pq.cnpq.br

[1] Departamento de Física, Universidade Federal Rural de Pernambuco, Rua Dom Manoel de Medeiros s/n, Dois Irmãos, 52171-900 Recife, PE, Brazil

[2] Departamento de Clínica e Odontologia Preventiva, Universidade Federal de Pernambuco, Av. Prof. Moraes Rego 1235, 50670-901 Recife, PE, Brazil

[3] Departamento de Ingeniería Eléctrica y de Computadoras, Universidad Nacional del Sur, B8000FWB, Bahía Blanca, Argentina

[4] Departamento de Estatística e Informática, Universidade Federal Rural de Pernambuco, Rua Dom Manoel de Medeiros s/n, Dois Irmãos, 52171-900 Recife, PE, Brazil

Introduction

Dental implant procedures have become increasingly common over the past decades, reaching the rate of a million operations per year [1], and clinical efficacy of over 95 %. The success rate of the treatment strongly depends on surface properties of titanium implants, and diverse techniques for implant preparation have been developed over the years [2], being widely implemented in commercial products. Nevertheless, there is still no clear consensus as to which of these treatments may lead to best long-term results, due to lack of standardized large scale in vitro and in vivo studies, together

with the current limited understanding of intricacies of the osseointegration phenomenon. In particular, the precise role of implant surface properties on the early stages of osseintegration is still not well understood.

There are several novel techniques for quantification of complexity, that have been introduced in the area of statistical physics, and subsequently successfully applied in a wide spectrum of other areas of knowledge [3–6], that may contribute to a better quantitative description of the early stages of osseointegration. Fractal dimension is a novel concept that has been increasingly employed in diverse areas of knowledge for quantifying the complexity of natural phenomena. Fractals are in fact commonly found in nature, being characterized by scale invariance and self-similarity, and have been used over the last decades for analysis of diverse phenomena in physiology and medicine, such as pulmonary emphysema [7] and heart rate [8]. The potential of fractal analysis was also explored in dentistry [9, 10]. In fact, only recently, fractal dimension has been used to quantify the surface roughness of dental implants and shown to be promising to differentiate between topological properties of dental implant surfaces obtained with different treatments [11–14].

However, fractal dimension is not always sufficient for describing an object, since rather different fractal objects may have the same fractal dimension. Lacunarity $\Lambda(r)$ [15] is another quantity that provides information about the distribution of voids and has been extensively used to complement the information contained in the concept of fractal dimension [3, 16, 17]. Finally, multifractals are objects that represent a composition of fractals with different individual fractal dimensions (monofractals), and therefore require description through a set of hierarchically distributed exponents, called multifractal spectrum. If this hierarchy of exponents is neglected, and the object is treated as a monofractal, the calculated dimension will assume some intermediate value [18]. Multifractals have been widely used in describing various phenomena in physiology and medicine [19, 20], ecology [21], and geophysics [22].

In the current work, we take a step beyond the fractal dimension approach that has been recently proposed for roughness quantification of dental surface images [12–14]. More precisely, we propose the use of yet more comprehensive measures: multifractal spectrum and lacunarity. We demonstrate the potential of these quantifiers to distinguish between complexity of implant surface scanning electron microscopy (SEM) images for different physiochemical treatments, before and after submersion in simulated body fluid (SBF). In particular, we study SEM images of machined titanium implant samples subjected to different combinations of sand blasting with aluminum oxide, etching with hydrofluoric acid, and treatment with calcium phosphate, before and after submersion in a simulated body fluid (SBF) for thirty days.

In the following section, we first describe the experiment and the used analytical methods (fractal dimension, multifractal spectrum, and lacunarity). In the subsequent section, we present the results of our analysis, and in the final section, we draw the conclusions.

Materials and Methods

Machined titanium implant samples were first subjected to different combinations of i) sand blasting with aluminum oxide, ii) etching with hydrofluoric acid, and iii) treatment with calcium phosphate [23], after which they were submersed in a simulated body fluid (SBF) [24] for 30 days. Magnified images of these samples were acquired through scanning electron microscopy (SEM), before and after SBF submersion, and binarized for posterior numerical analysis.

Simulated body fluid (SBF) solution was prepared at the Laboratory of Pharmacognosy of the Department of Pharmaceutical Sciences of the Universidade Federal de Pernambuco (UFPE), following the recipe provided by Kokubo and Takadama [24] (for the details on the preparation procedure, see Appendix A of [24]). The SBF chemical composition is given in Table 1.

The images at magnification of 200 were obtained by Scanning Electron Microscope JEOL 5600, (Japan), Voltage 10 kV, at the Physics Department of Universidade Federal de Pernambuco (UFPE). For each of the 16 available SEM images shown in Fig. 1, a rectangular region of interest (ROI) of 640 x 400 pixels is further analyzed numerically, using Mathlab and ImageJ software with FracLac package. The concepts of fractal dimension, lacunarity, and multifractal spectrum, analyzed numerically in the rest of this paper, are briefly described as follows.

Table 1 The chemical composition of the SBF solution

Reagent	Quanity	Purity (%)
NaCl	8.035 g	99.5
$NaHCO_3$	0.355 g	99.5
KCl	0.225 g	99.5
$K_2HPO_4\,3H_2O$	0.231 g	99.0
$MgCl_2\,6H_2O$	0.311 g	98.0
1.0 M-HCl	39 ml	–
$CaCl_2$	0.292 g	95.0
Na_2SO_4	0.072 g	99.0
Tris[a]	6.118 g	99.0
1.0 M-HCl	0–5 ml	–

[a] $(HOCH_2)_3CNH_2$ hydroxymethyl aminomethane

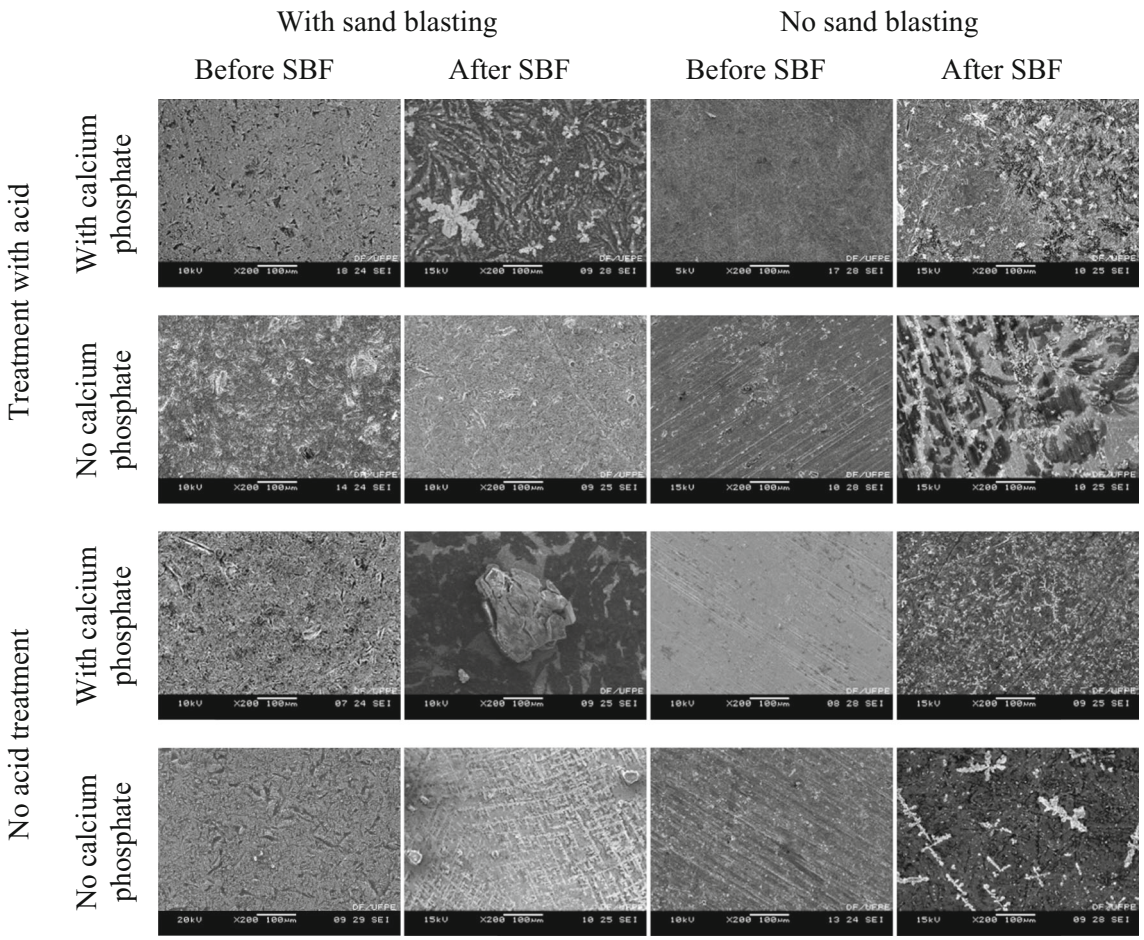

Fig. 1 SEM images of titanium implants for different treatment combinations, before and after SBF immersion

Fractal dimension

Various methods have been proposed up to date for calculating fractal dimension calculation, among which the box-counting method is the most widely used because of its simplicity and robustness [25], proceeding as follows. The structure to be analyzed is covered with a grid of varying size r, and for each grid size the number of nonempty grid boxes $n(r)$ are counted. For a self-similar fractal structure, the number of nonempty boxes should behave as $n(r) \sim r^{-Df}$, where D_f is the fractal dimension, and may be found from the expression

$$D_f = \lim_{r \to 0} \frac{\log n(r)}{\log(1/r)},$$

by estimating the slope of the linear regression of $\log n(r)$ versus $\log(1/r)$.

Lacunarity

A simple procedure to calculate the lacunarity [26, 27] for a binary image is as follows:

Table 2 Fractal dimension (standard deviation) of binarized images of dental implants with different treatments before and after SBF immersion

	With sand blasting		No sand blasting	
	Before SBF	After SBF	Before SBF	After SBF
Treatment with acid				
With calcium phosphate	1.919 (0.013)	1.859 (0.014)	1.924 (0.015)	1.920 (0.015)
No calcium phosphate	1.920 (0.013)	1.930 (0.015)	1.925 (0.011)	1.845 (0.013)
No acid treatment				
With calcium phosphate	1.917 (0.014)	1.693 (0.011)	1.925 (0.011)	1.881 (0.014)
No calcium phosphate	1.927 (0.014)	1.903 (0.014)	1.900 (0.014)	1.687 (0.012)

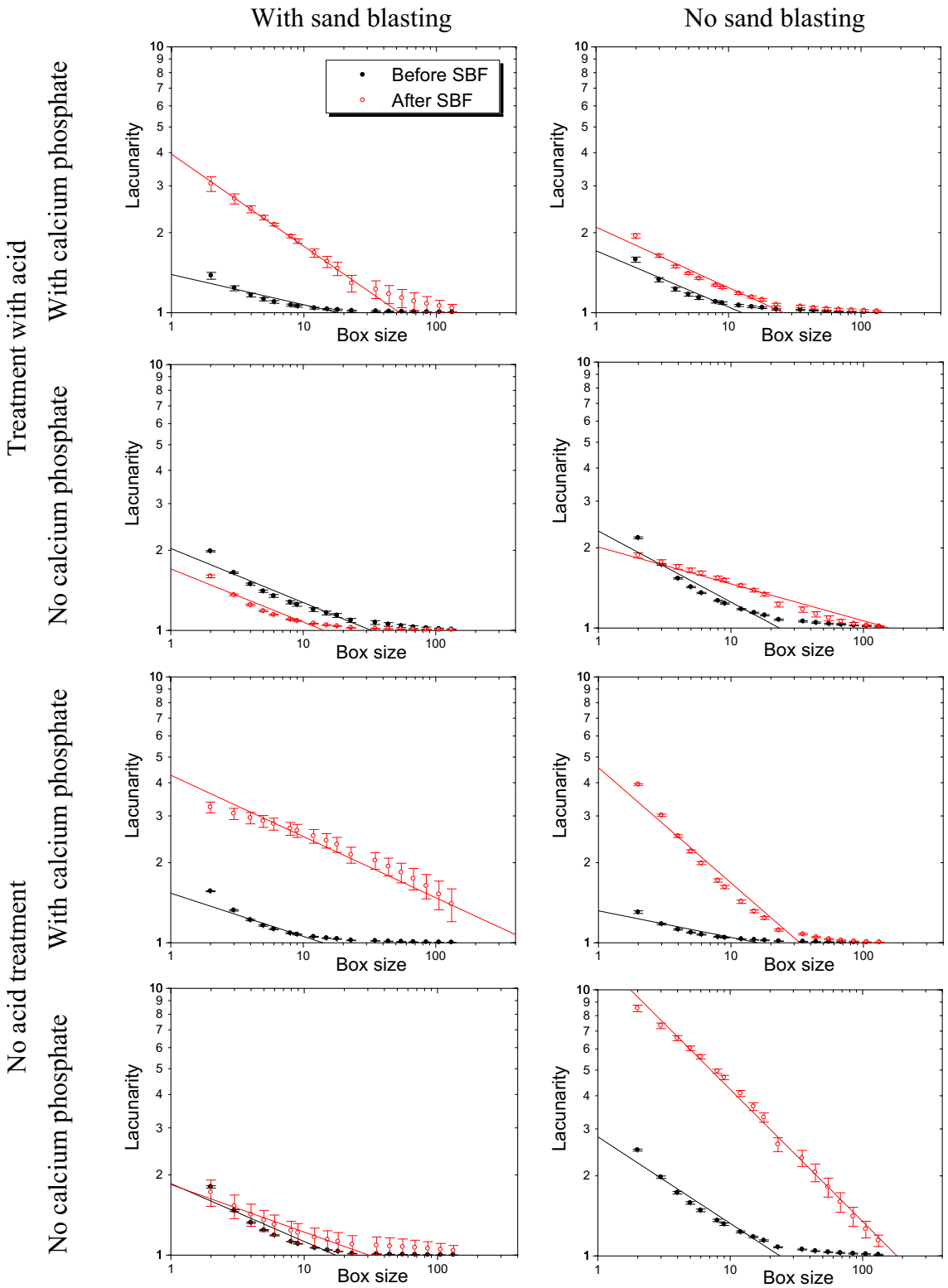

Fig. 2 Lacunarity of SEM images of titanium implants for different treatment combinations, before and after SBF immersion, on double logarithmic scale. Regression lines emphasize power law behavior before the homogeneity limit is reached (see text for more details)

i. A box of side *r* is placed on the upper left corner of the image, and the number *s* of black pixels within this box is counted;

ii. The box is moved one pixel position over the image, and the number of occupied boxes is counted again;

Table 3 lacunarity exponent β and the largest observed lacunarity value $\Lambda(2)$ of binarized images of dental implants with different treatments, before and after SBF immersion

	With sand blasting				No sand blasting			
	Before SBF		After SBF		Before SBF		After SBF	
	β	$\Lambda(2)$	β	$\Lambda(2)$	β	$\Lambda(2)$	β	$\Lambda(2)$
Treatment with acid								
With calcium phosphate	0.114	1.377	0.346	3.050	0.211	1.582	0.228	1.941
No calcium phosphate	0.204	1.985	0.200	1.598	0.267	2.182	0.139	1.875
No acid treatment								
With calcium phosphate	0.162	1.562	0.230	3.232	0.100	1.303	0.433	3.941
No calcium phosphate	0.217	1.803	0.178	1.718	0.325	2.500	0.496	8.519

iii. This process is repeated for all possible box positions, and thus the box occupation frequency distribution $n(s,r)$ of the boxes is obtained, together with the corresponding empirical probability distribution $Q(s,r)=n(s,r)/N(r)$, where $N(r)$ is the total number of boxes of size r.

iv. Lacunarity for the given box of side r is defined by:

$$\Lambda(r) = \frac{Z_2(r)}{[Z_1(r)]^2}$$

where $Z_1(r) = \sum_s s\, Q(s,\, r)$ and $Z_2(r) = \sum_s s^2 Q(s,\, r)$ are the first and second moment of the distribution $Q(s,r)$, respectively. In terms of the more common statistics, mean $\mu_r=Z_1(r)$ and standard deviation $\sigma_r = \sqrt{Z_2(r)} - [Z_1(r)]^2$, lacunarity is given by

$$\Lambda(r) = \frac{{\sigma_r}^2}{{\mu_r}^2} + 1.$$

It should be noted that reducing r leads to reduction of the mean occupation μ_r, thus increasing lacunarity $\Lambda(r)$, reflecting a larger number of gaps (empty boxes) in the image that occurs with scale reduction. In the other direction, increasing r leads to reduction of the box occupation standard deviation, until the "homogeneity limit" is reached (all boxes contain roughly the same number of pixels, and $(r)=1$. In general, the increasing frame size μ_r decreases lacunarity [28], and in some cases, this decrease follows a power law $\Lambda(r)\sim r^{-\beta}$, where the lacunarity exponent β can be calculated by linear regression of $\log(\Lambda(r))$ versus $\log(r)$, quantifying the rate of approach to the homogeneity limit (when further increase of r does not bring about further lacunarity reduction).

Multifractals

A direct method for calculating the multifractal spectrum, introduced by Chhabra and Jensen [29], for a binary image containing M black pixels on white background, proceeds as follows:

The image is covered with $N(r)$ boxes of linear size r, and the number of black pixels $M_i(r)$ within each box $i=1,\ldots,N(r)$ is counted, in order to calculate the probability $P_i(r)=M_i(r)/M$ that a randomly chosen black pixel belongs to the i-th box.

An independent continuous parameter q is now introduced to define probability measure

$$\mu_i(q,r) = \frac{[P_i(r)]^q}{\sum_{j=1}^{N(r)} [P_j(r)]^q}\ .$$

A set of q values is selected (typically in the range −10, 10), and for each value the Hausdorff dimension $f(q)$ is calculated as the slope of regression line of $\sum_i \mu_i(q,r)\ \log\mu_i(q,r)$ versus $\log r$

The singularity spectrum $\alpha(q)$ is calculated as the slope of regression line of $\sum_i \mu_i(q,r)\ \log P_i(r)$ versus $\log r$.

Pairs of points $f(q)$ and $\alpha(q)$ are used to construct the graph $f(\alpha)$.

Parameter q in the above described procedure serves as a "magnifying glass", where for $q>1$ high probability regions are enhanced, and for $q<1$ the low probability regions become dominant, while $\mu_i(1,r)$ coincides with the original probability $P_i(r)$. The resulting $f(\alpha)$ spectrum reveals wealth of information about the structure, and has the following properties:

If the analyzed structure is monofractal, $f(\alpha)$ collapses to a single point, otherwise, it represents a function with a single maximum (or "hump").

Point α_0 where $f(\alpha)$ is maximum corresponds to dominant singularity (value that would have been obtained for fractal dimension if multifractality was ignored and the structure treated as a monofractal).

- The left hand side of the spectrum corresponds to large fluctuations, and the right hand side to small fluctuations — asymmetry indicates prevalence of one, or the other.

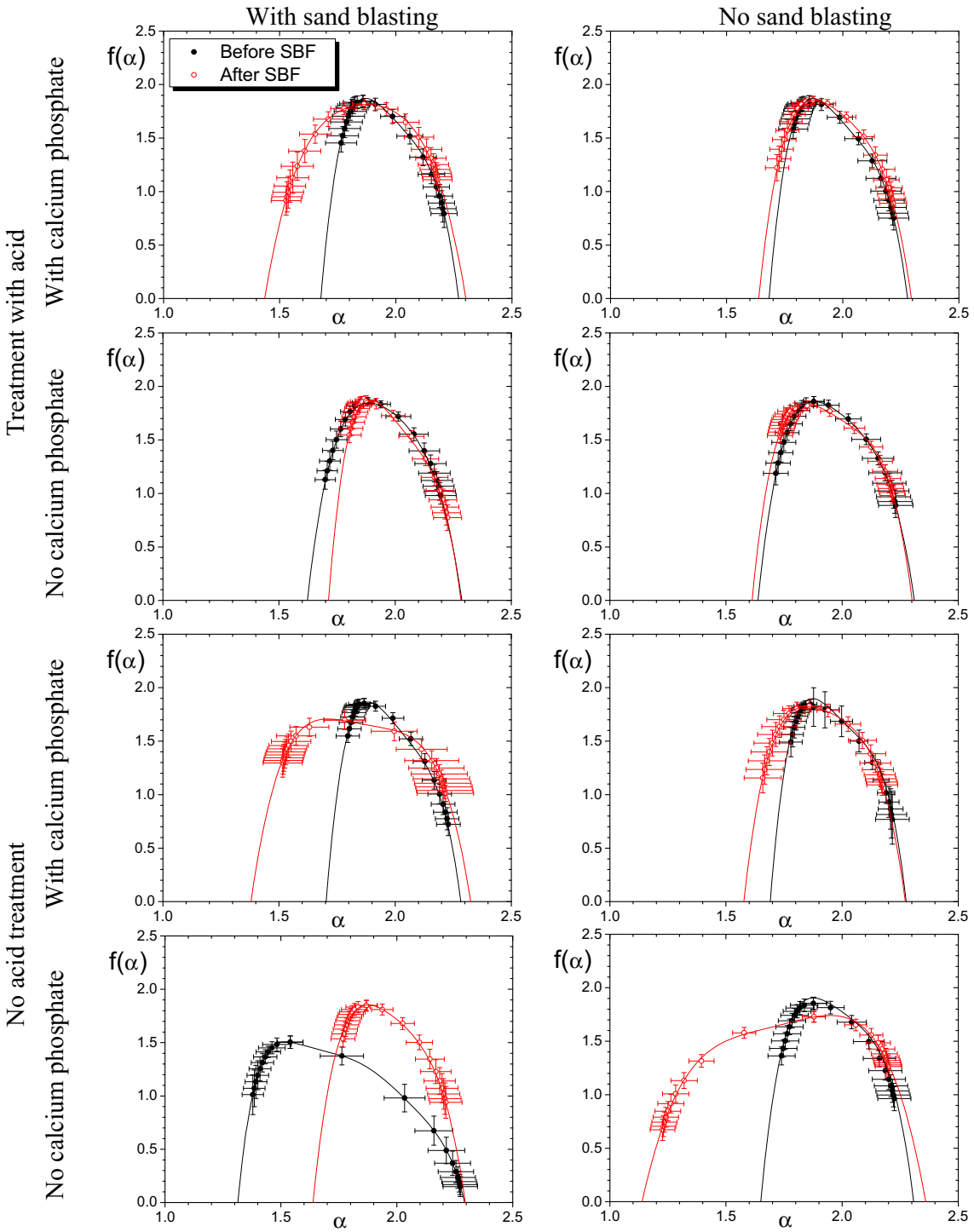

Fig. 3 Multifractal spectra of SEM images of titanium implants for different treatment combinations, before and after SBF immersion. The full lines represent regression to fourth order polynomials (see text for details)

- The width of the spectrum indicates degree of multifractality (weak or pronounced).

The collection of quantifiers described in this section is used in the rest of this work to perform an exploratory analysis of the early stages of osseointegration on the available experimental data, while in fact in the future, when systematic experimental data on the quality of implants with different treatments becomes more abundant, they may be used as a feature set for classification as "good" or "bad" implants through a neural network approach.

Table 4 Width w of multifractal spectra of dental implants with different treatments, before and after SBF immersion

	With sand blasting		No sand blasting	
	Before SBF	After SBF	Before SBF	After SBF
Treatment with acid				
With calcium phosphate	0.594	0.867	0.597	0.657
No calcium phosphate	0.665	0.570	0.674	0.689
No acid treatment				
With calcium phosphate	0.580	0.946	0.585	0.696
No calcium phosphate	0.979	0.621	0.659	1.222

Results and discussion

The large diversity of images on Fig. 1 both before and after SBF submersion demonstrates the complexity of the problem at hand. While the ultimate goal of implant treatment studies in general is to establish which treatments are the best (leading to long term stability of implants), this goal remains far from reach at the current level of understanding of the intricacies of osseointegration on titanium implants. The following quantitative exploratory analysis may help in paving the way for a deeper future understanding of this phenomenon.

Surfaces of implants subjected to different treatment combinations before SBF submersion show rather different roughness patterns (local distributions of protrusions and cavities). Nevertheless, the fractal dimension values presented in Table 2 indicate that in terms of overall complexity, they are all rather similar.

On the other hand, the same implants after SBF submersion and crystal formation, as reported previously [11], exhibit rather different fractal dimension values. For acid treatment, fractal dimension is (moderately) reduced if either both sand blasting and calcium phosphate treatment are also applied, or if neither of them is applied. For samples with no acid treatment, even stronger reduction of fractal dimension for these two cases (absence or presence of both sand blasting and calcium phosphate treatment) is observed.

Lacunarity analysis of all the available images is represented graphically in Fig. 2 where it is seen that lacunarity is increased after SBF treatment in all cases except for acid treatment with sand blasting before SBF immersion.

It is also seen from Fig. 2 that lacunarity follows the power law $\Lambda(r) \sim r^{-\beta}$ before the homogeneity limit is reached (when lacunarity drops to unity), while the rate of decay is increased (larger lacunarity exponent β) in four cases (acid+sand blasting+calcium phosphate; sand blasting+calcium phosphate; calcium phosphate; no treatment), it remains roughly the same in two cases (acid+calcium phosphate; acid+sand blasting), and is decreased when only acid treatment is applied. Numerical values for the lacunarity exponent β and the largest observed lacunarity value (for the smallest used box size $r=2$) are given in Table 3, for inspection.

Multifractal spectra of all the available images are represented graphically in Fig. 3 where it is seen that all the studied implants do indeed represent multifractals, rather than monofractals. In accordance with the previous observations about fractal dimension, multifractal spectra of implants for different treatments before submersion in SBF display rather similar spectra, where small fluctuations are more pronounced than large (more pronounced right hand side of the spectra). After submersion in SBF, the spectra in most cases become wider, where typically the large fluctuations (left hand side of the spectra) are enhanced. This effect is the most pronounced for i) acid treatment+sandblasting+calcium phosphate, ii) sand blasting+calcium phosphate, and iii) no treatment, where large crystal formations are observed in Fig. 1. The only exceptions are acid etching with sand blasting, and sand blasting without other treatments, where in fact fluctuations diminish after SBF immersion, which is reflected in shrinkage of the multifractal spectrum.

Finally, in Table 4 we present the numerical data for the width $w=\alpha_{max}-\alpha_{min}$ of multifractal spectra of all the implants, obtained by fitting the data on Fig. 3 to a fourth order polynomial form [30, 31] to estimate the values for α_{min} and α_{max} for each of the graphs. As mentioned before, these values reflect the degree of multifractality, and are provided here for quantitative comparison of different treatment combinations, before and after SBF immersion.

Conclusion

In this work we apply fractal, multifractal, and lacunarity analysis on binarized scanning electron microscopy images of titanium implants that were first subjected to different treatment combinations of i) sand blasting, ii) acid etching, and iii) exposition to calcium phosphate and were then submersed in a simulated corporal fluid for 30 days. All the three techniques are applied to the implants before and after SBF immersion, in order to provide a comprehensive set of common quantitative descriptors for both the complex cavity/protrusion spatial distributions observed after different treatment combinations,

and for the complexity of crystal patterns after SBF immersion, which emulates early stages of osseointegration.

Although the surfaces of implants subjected to different treatment combinations display visually rather different patterns, all three techniques yield rather similar results for different treatment combinations before SBF immersion. On the other hand, the three techniques yield rather different quantitative results after SBF immersion for different treatment combinations, reflecting the complexity and space filling property of the observed crystal structures (characterized by presence of large and small crystals, uniformly or locally deposited, of simple or dendritic shape).

While our analysis is not conclusive from a practical viewpoint (e.g., which treatment combination yields best implants), considering the large variety of possible treatments and a great number of their possible combinations (especially if they are also combined in different order, possibly producing different effects), future large-scale systematic in vivo studies should substantially benefit from the current quantitative description. More precisely, if the current analysis was performed in parallel with an in vivo study for a given (sufficiently large) number of treatment combinations, it may be expected that firm criteria could be established as to which surface roughness and SBF crystal complexity parameters are associated with the best in vivo results, thus diminishing the necessity of further in vivo studies.

Acknowledgments This work is supported by research grants from CNPq, CAPES and FACEPE (Brazilian research agencies), and MINCYT (Argentinean Ministry of Science, Technology and Productive Innovation).

Compliance with ethical standards

Conflict of interest The authors declare that they have no competing interests.

References

1. Layrolle P, Amouriq Y, Le Gunnec L, Soueidan A (2007) Surface treatments of titanium dental implants for rapid osseointegration. Dent Mater 23:844–854
2. Bagno A, Di Bello C (2004) Surface treatments and roughness properties of Ti-based biomaterials. J Mater Sci Mater Med 15: 935–949
3. Malhi Y, Román-Cuesta RM (2008) Analysis of lacunarity and scales of spatial homogeneity in IKONOS images of Amazonian tropical forest canopies. Remote Sens Environ 112:2074–2087
4. Velazquez-Camilo O, Bolaños-Reynoso E, Rodriguez E, Alvarez-Ramirez J (2010) Characterization of cane sugar crystallization using image fractal analysis. J Food Eng 100:77–84
5. Caniego FJ, Espejo R, Martin MA, San José F (2005) Multifractal scaling of soil spatial variability. Ecol Model 182:291–303
6. Sachs D, Lovejoy S, Schertzer D (2002) The multifractal scaling of cloud radiances from 1m to 1km. Fractals 10:253–257
7. Chung HW, Huang YH (2000) Fractal analysis of nuclear medicine images for the diagnosis of pulmonary emphysema. Am J Roentgenol 174:1055–1059
8. Goldberger AL, Amaral LAN, Hausdorff JM, Ivanov P, Peng CK, Stanley HE (2002) Fractal dynamics in physiology: alterations with disease and aging. PNAS 99:2466–2472
9. Sánchez I, Uzcátegui G (2011) Fractals in dentistry. J Dent 39:273–292
10. Updike SX, Nowzari H (2008) Fractal analysis of dental radiographs to detect periodontitis-induced trabecular changes. J Periodontal Res 43:658–664
11. dos Santos LCB, Carvalho AAT, Leao JC, Duarte-Neto PJ, Stosic T, Stosic B (2015) Fractal measure and microscopic modeling of osseointegration. Int J Prosthodont Restor Dent; accepted for publication
12. Perotti V, Aprile G, Degidi M, Piatelli A, Lezzi G (2011) Fractal analysis: a novel method to assess roughness organization of implant surface topography. Int J Prosthodont Restor Dent 31:633–639
13. Lezzi G, Aprile G, Tripodi D, Scarano A, Piatelli A, Perotti V (2012) Implant surface topographies analyzed using fractal dimension. Implant Dent 20:131–138
14. Ehrenfest D (2011) Fractal patterns applied to implant surface: definitions and perspectives. J Oral Implantol 37:506–509
15. Mandelbrot BB (1982) The fractal geomeytry of nature. Freeman, San Francisco
16. Zaia A, Eleonori R, Maponi P, Rossi R, Murri R (2006) MR imaging and osteoporosis: fractal lacunarity analysis of trabecular bone. IEEE Trans Inf Technol Biomed 10:484–489
17. Yasar F, Akqunlu F (2005) Fractal dimension and lacunarity of dental radiographs. Dentomaxillofacial Radiol 34:261–267
18. Feder J (1988) Fractals. Plenum Press, New York
19. Stosic T, Stosic B (2006) Multifractal analysis of human retinal vessels. IEEE Trans Med Imaging 25:1101–1107
20. Lopes R, Betrouni N (2009) Fractal and multifractal analysis: a review. Med Image Anal 13:634–649
21. L. Seuront, Fractals and multifractals in ecology and aquatic science, Taylor & Francis 2009, 400p
22. Lovejoy S, Schertzer D (2007) Scale, scaling and multifractals in geophysics: twenty years on. Nonlinear dynamics in Geosciences, Ed. A.A. Tsonis, J. Elsner, Springer, 311-337
23. Guo CY, Tang ATH, Matinlinna JP (2012) Insights into surface treatment methods of titanium dental implants. J Adhes Sci Technol 26:189–205
24. Kokubo T, Takadama H (2006) How useful is SBF in predicting in vivo bone bioactivity? Biomaterials 27:2907–2915
25. Theiller J (1990) Estimating fractal dimension. J Opt Soc Am 7: 1055–1073
26. Allain C, Cloitre M (1991) Characterizing the lacunarity of random and deterministic fractal sets. Phys Rev A 44:3552–3558
27. Plotnick RE, Gardner RH, Hargrove WW, Prestegaard K, Perlmutter M (1996) Lacunarity analysis: a general technique for the analysis of spatial patterns. Phys Rev E 53:5461–5468
28. Myint SW, Lam N (2005) A study of lacunarity-based texture analysis approaches to improve urban image classification. Comput Environ Urban Syst 29:501–523
29. Chhabra A, Jensn RV (1989) Direct determination of the f(α) singularity spectrum. Phys Rev Lett 62:1327–1330
30. Shimizu Y, Thurner S, Ehrenberger K (2002) Multifractal spectra as a measure of complexity in human posture. Fractals 10:103–116
31. de Benicio RB, Stosic T, de Figueiredo PH, Stosic B (2013) Multifractal behavior of wild-land and forest fire time series in Brazil. Phys A 392:6367–6374